

## THERMAL COMPTONIZATION IN GRS 1915+105

OSMI VILHU,<sup>1</sup> JURI POUTANEN,<sup>2</sup> PETTER NIKULA,<sup>1</sup> AND JUKKA NEVALAINEN<sup>3</sup>

*The Astrophysical Journal Letters, in press*

### ABSTRACT

The Rossi X-ray Timing Explorer (*RXTE*) data of GRS 1915+105 from several observing periods are modeled with a thermal Comptonization model. Best-fit models indicate that there is a strong correlation between the inner disk temperature and the disk luminosity. The hard Comptonized luminosity does not depend significantly on the total luminosity. The spectral hardness of the Comptonized radiation, the fraction of seed soft photons scattered by the Comptonizing cloud, its Thomson optical depth, and the fraction of the total power dissipated in the optically thin hot plasma, all strongly anticorrelate with the luminosity. We find that the inner disk radius is almost constant and that the hot Comptonizing corona shrinks at high luminosities. We note that the fits using XSPEC diskbb + power law model underestimate the amplitude of the blackbody component (and therefore the corresponding size of the emitting region) and overestimate the absorption column density and the total, corrected for absorption, luminosity.

*Subject headings:* accretion, accretion disks – binaries: close – black hole physics – radiation mechanisms: non-thermal – stars: individual (GRS 1915+105) – X-rays: binaries

### 1. INTRODUCTION

The X-ray transient GRS 1915+105 was discovered by Castro-Tirado et al. (1992) using the WATCH all-sky monitor on the *GRANAT* satellite. Since then it has been one of the most luminous X-ray sources in the sky. The *Rossi X-ray Timing Explorer* (*RXTE*) has been monitoring it frequently and a rich pattern of variability has emerged from these data with time scales from years down to 15 msec (see e.g., Morgan, Remillard, & Greiner 1997; Munro, Morgan, & Remillard 1999; Belloni et al. 2000). Often the overall spectral shape in the 2–50 keV energy range has been modeled with a disk blackbody accompanied by a power law tail (e.g. Belloni et al. 1997; Munro et al. 1999).

A power law, however, is not a good approximation to the Comptonization spectrum in the energy range close to the peak of the blackbody. This fact inspired us to use a thermal Comptonization code by Poutanen & Svensson (1996, PS96) to model the spectrum. Vilhu & Nevalainen (1998) applied a similar analysis to a selected set of observations of GRS 1915+105. A spherical geometry for the hot Comptonizing plasma cloud is assumed where the seed soft photons are coming from the surrounding cool disk which has some overlap with the central cloud (Poutanen, Krolik, & Ryde 1997). A geometry, with no overlap between the disk and the hot cloud (“corona”), can correspond to a physical situation when the central part of the disk is overheated (Beloborodov 1998) at large accretion rates. The central hot cloud can also be related to the innermost part of the jet. In the opposite situation, when there is a large overlap between the disk and corona, we arrive at a simple disk-corona model (e.g. Haardt & Maraschi 1993; Svensson & Zdziarski 1994; Stern et al. 1995). Physically this could correspond to the release of a large fraction of the total energy in the surface layers of the accretion disk, for example, due to annihilation of buoyant magnetic fields (e.g. Tout & Pringle 1992; Miller & Stone 2000). The adopted geometry is thus quite generic and it can represent well the X-ray emitting region in a number of

physical situations.

An important question is whether the energy distribution of electrons responsible for Comptonization is thermal or non-thermal. In Cygnus X-1, for example, when the spectrum is hard, electrons are mostly thermal (Gierliński et al. 1997; Poutanen 1998), while in the soft state, Comptonization probably proceeds in hybrid, thermal/non-thermal plasmas (Poutanen & Coppi 1998; Gierliński et al. 1999). The lower energy photons (below  $\sim 20$  keV) are produced mostly by a thermal population of electrons, and the high energy tail extending to  $\sim 1$  MeV is produced by single scattering off non-thermal electrons. Up to date, there are no detailed spectral studies of GRS 1915+105 using physical models. However, if one uses Cyg X-1 as an analogy, one can argue that thermal Comptonization probably dominates the spectra below 20–50 keV. In the present paper, a thermal Comptonization model is applied to the *RXTE* data of GRS 1915+105 collected from several observing intervals during 1996–1997.

### 2. OBSERVATIONS

We collected 36 Proportional Counter Array (PCA) and High-Energy X-ray Timing Experiment (HEXTE) observations of GRS 1915+105, performed during 1996–97, from the ‘production’ archive of *RXTE*, with typical observing times of a few hours. The selection procedure was rather random, its main purpose was to extract a sufficient number of low, medium and high luminosity states of the system. Figure 1 shows the ASM (All Sky Monitor) light curve with the selected PCA and HEXTE observations marked. The data with 128 (PCA Standard 2 data) and 64 (HEXTE) channels of spectral information and 16 s temporal resolution of five PCU’s (proportional counter units) and both HEXTE clusters were used. The background was subtracted (using PCAbackest and HEXTE rocking) although its effect is not crucial, since we limited the PCA and HEXTE spectra in the range 2–20 keV and 15–60 keV, respectively.

Inside each of the 36 observation periods the data were

<sup>1</sup>Observatory, Box 14, FIN-00014 University of Helsinki, Finland; osmi.vilhu@helsinki.fi; petter.nikula@helsinki.fi

<sup>2</sup>Stockholm Observatory, SE-133 36 Saltsjöbaden, Sweden; juri@astro.su.se

<sup>3</sup>ESA/ESTEC Astrophysics Division, Box 299, 2200 AG Noordwijk, The Netherlands; jnevalai@astro.estec.esa.nl

binned into separate luminosity groups (1–5) to accumulate a spectrum (using PCA count rate criterion), resulting in 101 individual spectra. Single spectra were used to represent the non-variable LULL-state observations (the long minimum phase in the middle of Fig. 1), while strongly oscillating observations were divided into 5 luminosity classes. These 5-class observations were 20402-01-33-00 (3000–26000 counts  $s^{-1}$ ,  $\kappa$ ), 20402-01-37-01 (3000–35000 counts  $s^{-1}$ ,  $\lambda$ ), 20402-01-43-00 (5000–45000 counts  $s^{-1}$ , mixed  $\beta$  and  $\mu$ ) and 20402-01-44-00 (5000–40000 counts  $s^{-1}$ ,  $\beta$ ) where the ranges of the five PCU’s count rates and the variability types by Belloni et al. (2000) are given in the parentheses. On the average a typical observation was split into three classes.

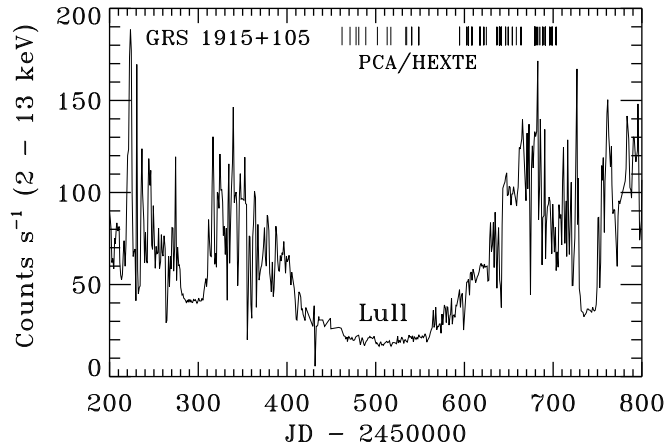


FIG. 1.— The ASM light curve (2–13 keV) of GRS 1915+105 with the PCA/HEXTE observations used in this paper marked with short vertical lines.

### 3. THE MODEL

The Comptonizing cloud (corona) is represented as a homogeneous sphere of radius  $R_c$  and Thomson optical depth  $\tau_T$ . The electrons in the cloud are assumed to have thermal distribution of temperature  $T_e$ . The optically thick disk supplying seed photons for Comptonization and penetrating into the central cloud has an inner radius  $R_{in} < R_c$ . Radiative transfer in the corona (Comptonization) is handled by the code of PS96 for a hemispherical geometry of the corona. In order to model the radiative transfer in a sphere, the boundary condition at the bottom of the hemisphere is modified. A photon crossing the bottom can be mirror-reflected instead of being absorbed by the disk (or Compton reflected) with the probability defined by the ratio  $R_{in}/R_c$  (Poutanen et al. 1997). The angle-dependent Compton reflection from the disk of neutral material is computed using Green’s function of Magdziarz & Zdziarski (1995).

The radial dependence of the disk temperature is that of the classical viscous disk  $T_{bb}(r) = T_{in}(r/R_c)^{-3/4}$  at  $r > R_c$  and  $T_{bb}(r) = T_{in}$  inside the coronal region (between  $R_{in}$  and  $R_c$ ). There are a few reasons why such a temperature profile is chosen. First, if a large fraction of the total power is dissipated in a corona which has large scale-height and covers a significant part of the inner cold disk, the reprocessing of coronal hard X-rays can produce a rather flat temperature profile. Second, owing to the stress-free inner boundary condition at the marginally stable orbit, the temperature profile even in a standard disk is rather flat between  $3R_g$  and  $10R_g$  (where  $R_g = 2GM/c^2$ ). Third, if  $R_{in}/R_c \rightarrow 0$ , the  $r^{-3/4}$  profile diverges. Regarding spectral fitting, the actual temperature profile makes little difference. The local spectrum was assumed to be a blackbody.

The total spectrum contains a blackbody-type component, a Comptonized tail and a Compton reflection component. To obtain both  $T_e$  and  $\tau_T$  is beyond the *RXTE* capability, therefore we fixed  $kT_e$  at 70 keV (but also made numerous fits with  $kT_e = 30$  keV and 150 keV). Instead of  $\tau_T$ , we then used the  $y$ -parameter ( $y = 4\tau_T\Theta$ , where  $\Theta = kT_e/m_e c^2$ ) which determines the spectral slope. Thus, the free parameters of the model are  $R_{in}/R_c$ ,  $y$  and  $T_{in}$ . The inclination  $i = 70^\circ$  was used, assuming that the radio jet is perpendicular to the disk (Mirabel & Rodríguez 1994). The important fact to notice is that the relative normalization between the disk and the Comptonized components is not free, but is a function of the model parameters mostly depending on  $\tau_T$  (or  $y$ ) and  $R_{in}/R_c$ .

### 4. RESULTS

The PCA/HEXTE spectra of GRS 1915+105 were fitted using XSPEC v.10 (Arnaud 1996), and allowing 2% systematic errors. The reduced  $\chi^2$ -values are less than 2.2 in all data sets, less than 1.6 in 64 sets, and less than 1.2 in 32 sets (for 132 degrees of freedom using 138 energy bins). The neutral hydrogen column density  $N_H$  was frozen at  $2.3 \times 10^{22} \text{ cm}^{-2}$ . This value is the best acceptable common value for spectra with high, intermediate and low luminosities. It is lower than that used in many previous works (e.g. Munro et al. 1999 used  $N_H = 6.0 \times 10^{22} \text{ cm}^{-2}$ ). However, our value is close to the galactic  $N_H$  in the direction of GRS 1915+105 (using Dickey & Lockman 1990 data, ftools/nh gives  $N_H = 1.75 \times 10^{22} \text{ cm}^{-2}$ , see also Rodríguez et al. 1994). The normalization factor between PCA and HEXTE data was allowed to vary freely, with the best-fit always giving HEXTE/PCA =  $0.70 \pm 0.05$ .

Figure 2 shows the best-fit results as a function of the disk luminosity  $L_{disk}$  (assuming a distance of 12.5 kpc, see Chaty et al. 1996; Fender et al. 1999) which was computed from the blackbody flux corrected for scattering in the corona and the  $\cos i$  angular dependence of the disk luminosity.  $L_{disk}$  and  $T_{in}$  together then determine the physical size of the system  $R_{in}$  and  $R_c$  (assuming blackbody emission). The hard luminosity,  $L_{hard}$ , is computed from the (approximately isotropic) flux in the Comptonized component (plus reflection).

The inner disk temperature  $T_{in}$  and  $R_{in}/R_c$  strongly correlate with the disk luminosity (Figs. 2a, d). The coronal  $y$ -parameter anticorrelates with  $L_{disk}$  depending on  $\ln L_{disk}$  nearly linearly (Fig. 2b). For low  $L_{disk}$ , the spectra are hard, and for large  $L_{disk}$  the spectra are soft. The hard Comptonized luminosity,  $L_{hard}$ , is relatively constant and in some cases of large  $L_{disk}$  significantly decreases (Fig. 2f). The geometry of the system (determined by the ratio  $R_{in}/R_c$ ) changes dramatically when  $L_{disk}$  varies. For large  $L_{disk}$ , the normalization of the Comptonized component decreases relative to the disk component, leading to  $R_{in}/R_c \sim 1$ . In our model,  $R_{in}/R_c \rightarrow 1$  means that only a small fraction  $\sim 3\%$  of soft disk photons are getting Comptonized, while the majority reaches the observer directly. We would not advise to take the ratios  $R_{in}/R_c$  at their face value since we made an assumption of a constant  $T_e$  (see § 5). One can conclude, however, that the number of soft photons that are intercepted by the corona (“scattered fraction”) decreases dramatically when  $L_{disk}$  increases.

The inner disk radius (Fig. 2e) is rather constant (25–40 km, without relativistic and color corrections). However, in two observations (20402-01-43-00 and 20402-01-44-00) the radii increased above 50 km during their lowest luminosity phases (‘downs’ in Fig. 2e, while ‘ups’ in Fig. 2e represent their high

luminosity phases). These two particular observations have  $\beta$ -type light curves (see Fig. 2X in Belloni et al. 2000) where the long minimum phases last 10–15 min (mini-lulls). It is interesting to note that these two observations preceded by 10 days those by Mirabel et al. (1998) with a similar light curve during which ejections of weak jets were discovered (seen in IR and radio).

To permit a comparison with models using a power law, we also fitted all our spectra with the ‘wabs + diskbb + powerlaw’ model of XSPEC (which we call the power law model hereafter) fixing  $N_{\text{H}} = 4.5 \times 10^{22} \text{ cm}^{-2}$ . The best-fit power law photon index,  $\Gamma$ , is shown in Fig. 2c. One sees an anticorrelation between  $\Gamma$  and  $y$ -parameter which is well represented by the relation  $\Gamma = 9/(4y^{2/9})$  (Beloborodov 1999).

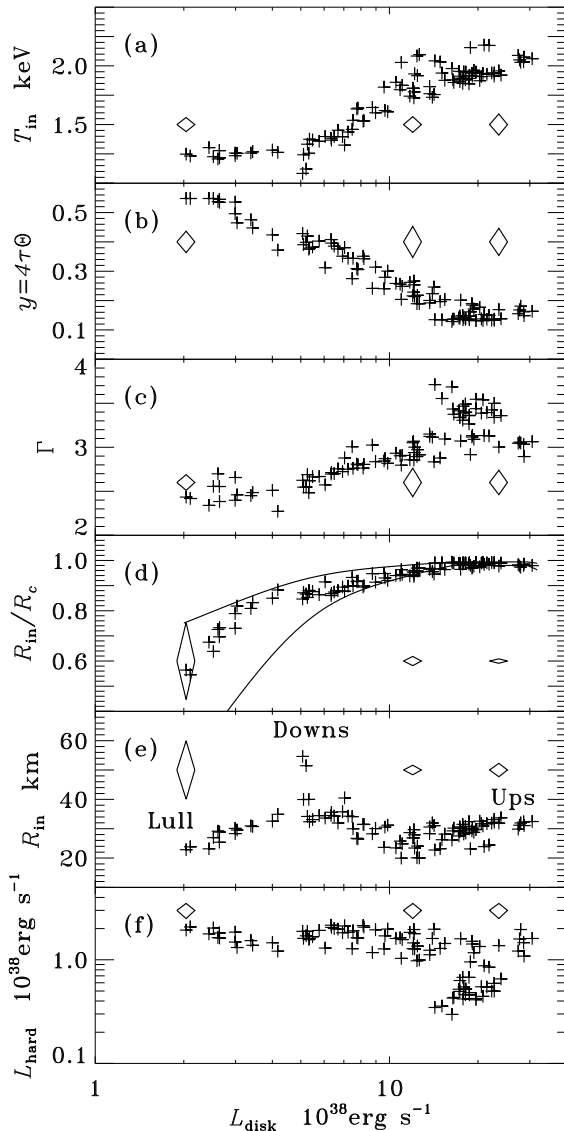


FIG. 2.— The best-fit results as functions of the disk luminosity,  $L_{\text{disk}}$ . The typical  $1\sigma$  error bars are shown by diamonds. The coronal temperature was fixed to  $kT_e = 70 \text{ keV}$ . The solid curves in panel (d) show the systematic effect for  $kT_e = 30 \text{ keV}$  (upper) and  $kT_e = 150 \text{ keV}$  (lower).

To illustrate the difference between the Comptonization and the power law models, we show the data for two observations together with the model spectra in Figure 3. (A gaussian line at 6.4 keV is added to both models.) We note that the power law model strongly overestimates the low energy part of the hard

component, and therefore strongly underestimates the amplitude of the blackbody component (dotted curves). For example, the amplitude of the blackbody in the power law fit is by a factor of four too low in the upper panels (marked Lull). Another strong effect is the difference in the  $N_{\text{H}}$  determined with the two models. Since the power law continues to low energies without a cutoff, the best fit  $N_{\text{H}}$  is  $(6 - 7) \times 10^{22} \text{ cm}^{-2}$ , while for the Comptonization model  $N_{\text{H}} \sim 2.5 \times 10^{22} \text{ cm}^{-2}$ . The power law model overestimates the total, corrected for absorption, luminosity if one extrapolates the model spectrum to low energies and gives also a poorer fit to the hard Lull-spectrum (compare left and right panels in Fig. 3).

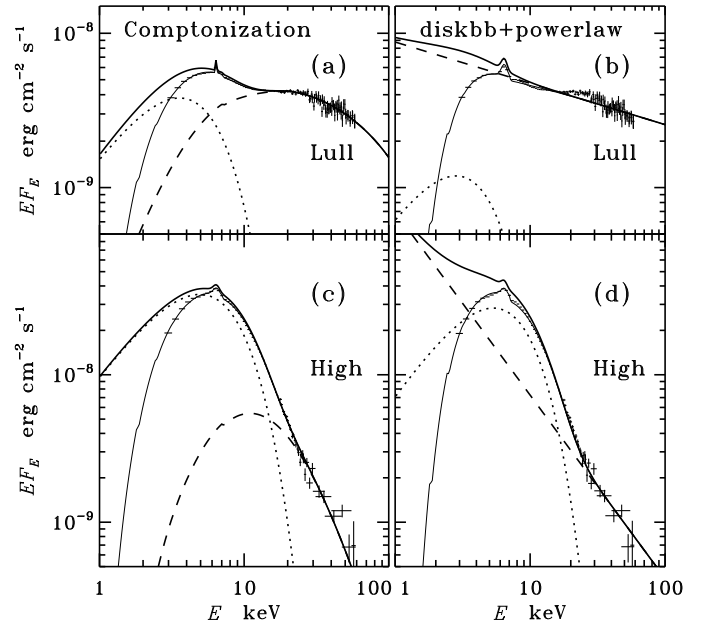


FIG. 3.— Examples of the observed spectra,  $E F_E$ , of GRS 1915+105 in the ‘Lull-phase’ (1997 February 22) and in the ‘High-phase’ (1997 June 18). The *RXTE* data are shown by crosses (the *HEXTE* data are rescaled to the PCA data). The best-fit Comptonization model spectra are shown by thin solid curves in panels (a) and (c). The disk blackbody, the Comptonized (plus Compton reflection) component, and the total spectrum are shown by dotted, dashed, and thick solid curves, respectively (in all the absorption is removed). The best-fit diskbb + powerlaw model spectra are shown in panels (b) and (d) by thin solid curves. Here the disk blackbody, the power law, and the total spectrum are shown by dotted, dashed, and thick solid curves, respectively (with absorption removed). See text for details.

## 5. DISCUSSION AND CONCLUSIONS

A strong correlation between the ratio  $R_{\text{in}}/R_c$  and the luminosity  $L_{\text{disk}}$  means that the coronal size  $R_c$  decreases when  $L_{\text{disk}}$  increases (since  $R_{\text{in}} \approx \text{const}$ ). Physically this means that the range of the disk surface where energy is dissipated in the optically thin phase (corona) shrinks. When spectra are relatively hard, the geometry of the system is similar to a disk-corona. For large  $L_{\text{disk}}$  and softer spectra, the Comptonizing plasma does not cover the disk. One can speculate that in this case hard X-rays are produced in the innermost part of the jet-like structure within the disk inner radius.

We cannot be certain, however, that the change in the geometry (i.e.  $R_{\text{in}}/R_c$ ) obtained from the fitting is real. The problem is that we assumed a constant  $T_e$  (since the *RXTE* data do not allow us to determine  $T_e$  unambiguously). If one fixes  $T_e$  at another value, the result does not change qualitatively (see Fig. 2d where a systematic effect on  $R_{\text{in}}/R_c$  is shown by the

solid curves for  $kT_e = 30$  keV and 150 keV). However, if  $T_e$  is allowed to vary the situation changes.

Let us consider a case of large  $L_{\text{disk}}$  when  $R_{\text{in}}/R_c \approx 1$  and  $\tau_T \approx 0.25$  (for  $kT_e = 70$  keV). In this case only about 3% of soft disk photons are scattered in the corona. The same fraction is scattered also if  $R_{\text{in}}/R_c = 0.5$  (here about 1/4 of soft photons are produced within the corona) and  $\tau_T \approx 0.03$ . Then the normalization of the Comptonized spectrum relative to the blackbody emission is about the same. The spectral shape does not change much since for small optical depths and mildly relativistic temperatures the contribution of multiply scattered photons is small. Therefore, the electron temperature has to increase to only about 90 keV in order to produce a similar Comptonized spectrum in the 3–70 keV energy range. From this analysis we can only conclude that the scattered fraction decreases when  $L_{\text{disk}}$  increases. If the geometry of the system does not change, i.e.  $R_{\text{in}}/R_c = \text{constant}$ ,  $\tau_T$  should decrease much more than is shown in Fig. 2b. One should note that this discussion is meaningful only if the spectra are indeed produced by thermal Comptonization.

Our choice of the disk temperature profile ( $T_{\text{bb}}$  is constant inside the corona) has also some (small) effect on  $R_{\text{in}}/R_c$ , while the effect is completely negligible for other fitting parameters. For the most extreme hard spectra (marked Lull) when  $R_{\text{in}}/R_c = 0.5$ , the number of seed photons is doubled if the peak temperature is reached at  $R_{\text{in}}$  (instead of  $R_c$ ), so that  $\tau_T$  should be smaller by a factor of 2 in order to produce similar spectra.

The mass accretion rate in GRS 1915+105 is high amounting to  $(0.1 - 1.5) \times \dot{M}_{\text{Edd}}$  (for a  $10M_\odot$  black hole), where  $\dot{M}_{\text{Edd}} = 10L_{\text{Edd}}/c^2 = 1.39 \times 10^{18} M/M_\odot \text{ g s}^{-1}$  corresponds to a radiative efficiency of 0.1. The inner disk radius lies in a rather narrow range of 25–40 km and the soft and hard state radii do not differ considerably.

One should be cautious with the absolute  $R_{\text{in}}$ -values derived, since relativistic and color corrections can be large. Using the results by Zhang et al. (1997) at inclination  $70^\circ$ , one obtains

the factors 1.23 and 1.07 for a non-rotating and an extreme prograde Kerr hole, respectively, by which the radii in Fig. 2e should be multiplied to obtain the innermost radius of the disk. After these corrections the mass of GRS 1915+105 should be smaller than  $4M_\odot$  and  $22M_\odot$  for a non-rotating and an extreme prograde Kerr hole, if the average radius derived (30 km in Fig. 2e) equals the last marginally stable orbit ( $3R_g$  and  $0.5R_g$  for a non-rotating and Kerr hole, respectively).

In conclusion, the *RXTE* data of GRS 1915+105 in a broad luminosity range  $(2 - 30) \times 10^{38} \text{ erg s}^{-1}$  can be modeled with a thermal Comptonization model. We find a strong correlation between the spectral slope, the disk temperature, and the disk luminosity  $L_{\text{disk}}$ . The hard Comptonized luminosity decreases somewhat when the total luminosity increases (meaning that the fraction of total power dissipated in an optically thin plasma decreases substantially with luminosity). The scattered fraction of seed soft photons and the optical depth of the Comptonizing plasma decrease with  $L_{\text{disk}}$ . There are indications that the size of the corona  $R_c$  shrinks at large luminosities, but this can be mimicked by corresponding changes in the optical depth. Detailed modeling of the broadband spectra (at least up to 300 keV) is needed to discriminate between those possibilities. The biggest question is, however, whether a pure *thermal* Comptonization model is applicable to GRS 1915+105.

Finally, we would like to point out that spectral fits using XSPEC diskbb + power law model underestimate the amplitude of the blackbody component and therefore the corresponding size of the emitting region. This model also overestimates the absorption column density and the luminosity corrected for absorption.

This research has been supported by the Academy of Finland (OV) and the Swedish Natural Science Research Council and the Anna-Greta and Holger Crafoord Fund (JP). JN acknowledges the grant from ESA. We thank Diana Hannikainen for reading the manuscript and the anonymous referee for valuable criticism and comments.

## REFERENCES

- Arnaud, K. A. 1996, in ASP Conf. Series Vol. 101, *Astronomical Data Analysis Software and Systems V*, ed. Jacoby G. H. & Barnes J. (San Francisco: ASP), 17
- Belloni, T., Mendez, M., King, A. R., van der Klis, M., & van Paradijs, J. 1997, *ApJ*, 488, L109
- Belloni, T., Klein-Volt, M., Mendez, M., van der Klis, M., & van Paradijs, J. 2000, *A&A*, 355, 271
- Beloborodov, A. M. 1998, *MNRAS*, 297, 739
- Beloborodov, A. M. 1999, in ASP Conf. Ser. 161, *High Energy Processes in Accreting Black Holes*, ed. J. Poutanen, R. Svensson (San Francisco: ASP), 295
- Castro-Tirado, A. J., Brandt, S., & Lund, N. 1992, *IAU Circ.* 5590
- Chaty, S., Mirabel, I. F., Duc, P. A., Wink, J. E., & Rodríguez, L. F. 1996, *A&A*, 310, 825
- Dickey, J., & Lockman, F. 1990, *ARA&A*, 28, 215
- Fender, R. P., Garrington, S. T., McKay, D. J., Muxlow, T. W. B., Pooley, G. G., Spencer, R. E., Stirling, A. M., & Waltman, E. B. 1999, *MNRAS*, 304, 865
- Gierliński, M., Zdziarski, A. A., Done, C., Johnson, W. N., Ebisawa, K., Ueda, Y., Haardt, F., & Philips, B. F. 1997, *MNRAS*, 288, 958
- Gierliński, M., Zdziarski, A. A., Poutanen, J., Coppi, P. S., Ebisawa, K., & Johnson, W. N. 1999, *MNRAS*, 309, 496
- Haardt, F., & Maraschi, L. 1993, *ApJ*, 413, 507
- Magdziarz, P., & Zdziarski, A. A. 1995, *MNRAS*, 273, 837
- Miller, K. A., & Stone, J. M. 2000, *ApJ*, 534, 398
- Mirabel, I. F., & Rodríguez, L. F. 1994, *Nature*, 371, 46
- Mirabel, I. F., Dhawan, V., Chaty, S., Rodríguez, L. F., Martí, J., Robinson, C. R., Swank, J., & Geballe, T. 1998, *A&A*, 330, L9
- Morgan, E., Remillard, R. A., & Greiner, J. 1997, *ApJ*, 482, 993
- Muno, M. P., Morgan, E. H., & Remillard, R. A. 1999, *ApJ*, 527, 321
- Poutanen, J. 1998, in *Theory of Black Hole Accretion Discs*, ed. M. A. Abramowicz, G. Björnsson, & J. E. Pringle (Cambridge: Cambridge Univ. Press), 100
- Poutanen, J., & Coppi, P. S. 1998, *Physica Scripta*, T77, 57
- Poutanen, J., & Svensson, R. 1996, *ApJ*, 470, 249 (PS96)
- Poutanen, J., Krolik, J. H., & Ryde, F. 1997, *MNRAS*, 292, L21
- Rodríguez, L. F., Gerard, E., Mirabel, I. F., Gómez Y., & Velázquez, A. 1994, *ApJS*, 101, 173
- Stern, B. E., Poutanen, J., Svensson, R., Sikora, M., & Begelman, M. C. 1995, *ApJ*, 449, L13
- Svensson, R., & Zdziarski, A. A. 1994, *ApJ*, 436, 599
- Tout, C. A., & Pringle, J. E. 1992, *MNRAS*, 259, 604
- Vilhu, O., & Nevalainen, J. 1998, *ApJ*, 508, L89
- Zhang, S. N., Cui, W., & Chen, W. 1997, *ApJ*, 482, L155